Journal of Alloys and Compounds 527 (2012) 176–183

Contents lists available at SciVerse ScienceDirect

Journal of Alloys and Compounds

journal homepage: www.elsevier.com/locate/jallcom

Primary α phase and its effect on the impact ductility of a high Cr content cast Ni-base superalloy

Liang Zheng*, Chengbo Xiao, Guoqing Zhang, Bo Han, Dingzhong Tang

Science and Technology on Advanced High Temperature Structural Materials Laboratory, Beijing Institute of Aeronautical Materials, Beijing 100095, China

ARTICLE INFO

Article history:
Received 11 January 2012
Received in revised form 16 February 2012
Accepted 19 February 2012
Available online xxx

Keywords:
High-temperature alloys
K4648
Microstructure
Mechanical properties
Phase transformation
Primary α-(Cr,Ni) phase

ABSTRACT

A high Cr content cast Ni-base superalloy, K4648, which contains 32–35 wt.% chromium, was prepared by vacuum induction melting, and poured into testing bars or heavy section specimens. The as-cast, heat treated and fractured specimens were investigated by optical metallography, quantitative metallography, X-ray diffraction (XRD), scanning electron microscopy (SEM) and energy dispersive spectroscopy (EDS). The isothermal solidification followed quenching (ISQ) technique and differential scanning calorimeter (DSC) experiments were also carried out. The result indicated that the primary α phase precipitated from the residual liquid in interdendritic region at 1190 °C near the solidus temperature. This phase can be represented as α-(Cr,Ni) in K4648 alloy because it solid solutionized by about 30 at.% of element Ni. The Vickers microhardness value of primary α phase is 6.3 GPa relative to 1.9 GPa of the γ matrix at the load of 0.2 N. This phase is brittle and tends to crack due to stress concentration during the solidification process. The primary α phase solutionized or transformed into $M_{23}C_6$ carbides during solid solution treatment in the range of 1180–1220 °C. However, small amounts of α phase remained even at the obvious incipient melting temperature of 1200–1220 °C. Therefore, primary α phase must be controlled during solidification process. The faster cooling during solidification process can decrease the amount of primary α phase in both as-cast and heat-treated K4648 alloys. Specimens cut from slow cooling heavy section castings with large amount of primary α phase possessed an impact ductility of 13.9 J/cm^2, which is much lower than 35.4 J/cm^2 of samples from faster cooling thin section testing bars. The extensive cracked α phase or transformed $M_{23}C_6$ carbides can be observed at the fracture surfaces and longitudinal sections of impact specimens. Large blocky primary α phase with a network-like distribution, forming as a result of slow cooling, has detrimental effects on the impact ductility of K4648 alloy and it is difficult to completely remove by heat treatment. Proper parameter to obtain faster cooling in the solidification of the alloy must be considered to avoid the detrimental primary α phase precipitation.

1. Introduction

The Ni-base superalloys have been widely used for producing crucial parts of gas turbine engines for over 50 years, thereby having been drawing extensive research over many various fields of study [1–11]. Chromium commonly exists in nickel-based superalloys due to the protective effects of Cr against hot corrosion and high temperature oxidation. In recent years, a high Cr content cast Ni-base superalloy, K4648, which contains 32–35 wt.% chromium, has been employed to manufacture advanced gas turbine engines. This alloy currently contains the highest Cr level in applied Ni-base superalloys, and possesses high degree of hot corrosion resistance, weldability, and lower cost relative to the Co-base superalloys. Although the microstructures and properties of high Cr content wrought superalloys have been investigated [12–14], studies of cast 32–35 wt.% high Cr alloys have been limited.

Currently, K4648 alloy is widely used in manufacturing large size complex integral castings in gas turbines, such as diffuser and vector jet nozzle components. However, this alloy suffered from low impact ductility in some cases. The authors have recently shown that the large blocky primary α phase tended to precipitate from liquid phase in the grain boundary or interdendritic region of as-cast specimens and proposed this as an explanation for the decrease in impact ductility of K4648 alloy. The primary α phase, which is rich in chromium and iron and with a body centered cubic (BCC) structure, has been proved to be harmful to the ductility, toughness, and corrosion resistance properties of stainless steels [15]. The impact strength drop was found to be correlated with the precipitation of secondary α-Cr phase at the grain boundaries of the wrought superalloy IN718 [16]. This phase has been demonstrated to form after long time exposure at 623–704 °C [17].

* Corresponding author at: P.O. BOX 81-1, Beijing 100095, China.
Tel.: +86 10 62496360.
E-mail addresses: zheng_liang@tom.com, leon.zhengliang@gmail.com (L. Zheng).

0925-8388/$ – see front matter © 2012 Elsevier B.V. All rights reserved.
doi:10.1016/j.jallcom.2012.02.166

Table 1
Chemical compositions of K4648 alloy.

	Cr	W	Mo	Nb	Ti	Al	C	Ce	B	Y	Ca	Ni
wt.%	33.66	4.86	2.90	0.90	0.92	0.94	0.067	≤0.03	≤0.008	≤0.04	≤0.02	Bal.
at.%	37.55	1.53	1.75	0.56	1.11	2.02	0.32	≤0.01	≤0.043	≤0.03	≤0.03	Bal.

Note: contents of element Ce, B, Y and Ca were not detected.

Moreover, the rod-like α-Cr phase precipitated in the interdendritic region of a single crystal superalloy DD8 during thermal exposure [18]. In author's previous work, similar structural primary α phase precipitation from liquid in late solidification of a high W content cast Ni-base superalloy has been shown [19]. However, the cause of primary α phase formation in as-cast high Cr content Ni-base superalloys and its effect on mechanical properties remain to be characterized.

In this paper, we investigated the characteristics, formation, and transformation of the primary α phase and its effect on the impact ductility in the high Cr content cast Ni-base superalloy K4648. The elucidation of the mechanisms involved in primary α formation may improve the impact ductility of high Cr content Ni-base superalloy.

2. Materials and experimental procedures

The analyzed composition of K4648 alloy is given in Table 1. The specimens used in this investigation were cut from testing bars or large section castings which were remelted and poured by K4648 master alloy ingots. In order to understand the effect of the cooling rate during solidification on the as-cast microstructure of alloy, the section size of the sample covered from 10 × 10 mm impact testing bar to 40 × 60 mm heavy section casting. Isothermal solidification followed quenching (ISQ) experiments were conducted to understand the solidification process of alloy. The ISQ technique is an effective method to determine the phase-specific precipitation temperatures and the liquid residual volume fraction and has been reported in previous works [20–23]. In this investigation, samples sizes of 5 × 5 × 10 mm^3 were cut from as-cast master alloy ingot, surrounded by slurry made of alumina powder and silicasol, and embedded into graphite blocks with existing drill holes. This packaging protected the melted alloy from flowing out and oxidizing. The blocks with embedded samples were heated up to 1360 °C and held for 10 min to allow full remelting. This was followed by cooling to different isothermal temperature in the range of 1350–1150 °C at rate of 10 °C/min and quenching with water to determine the precipitation temperature of primary α phase. The composition of primary α phase and the segregation of Cr between solid and frozen liquid phase during isothermal solidification were detected by energy dispersive spectroscopy (EDS). Differential scanning calorimeter (DSC) experiments was carried out using a NETZSCH STA 409C analyzer to determine the precipitation temperatures range of the phases. The rates of heating and cooling were set at 10 °C/min. The as-cast specimens with different section sizes were solid solutionized at 1180–1220 °C for 1–2 h and 1180 °C/4 h to examine the solution and the transformation of the primary α phase. The α phase and transformed $M_{23}C_6$ carbides was distinguished by a 10 g potash prussiate + 10 g NaOH + 100 ml H_2O solution etching. Impact test was carried out on samples cut from a K4648 testing bar and heavy section casting, which have been heat treated at 1180 °C/4 h A.C. + 900 °C/16 h A.C. The fracture surfaces and longitudinal sections of impact specimens were investigated by scanning electron microscopy (SEM) to explore the effects of primary α phase on impact ductility. Electrolytic extraction of minor phases in as-cast K4648 alloy was performed in a Methanol solution containing 10% HCl at a voltage of 6 V for 2 h. The extracted residues were identified using a D8 advanced X-ray Diffractometer (XRD). The microstructure of K4648 alloy was revealed by 10 ml HNO_3 + 30 ml HCl chemical etching or by electrolytic etching in 15%H_2SO_4–methanol solution and analyzed by optical metallography (OM), quantitative metallography (QM), scanning electron microscopy (SEM), and energy dispersive spectrum (EDS).

3. Results and discussion

3.1. Primary α phase and its characteristics in as-cast microstructure of K4648 alloy

The as-cast microstructure of K4648 alloy is presented in Fig. 1. A dendritic structure is evident in all specimens, with

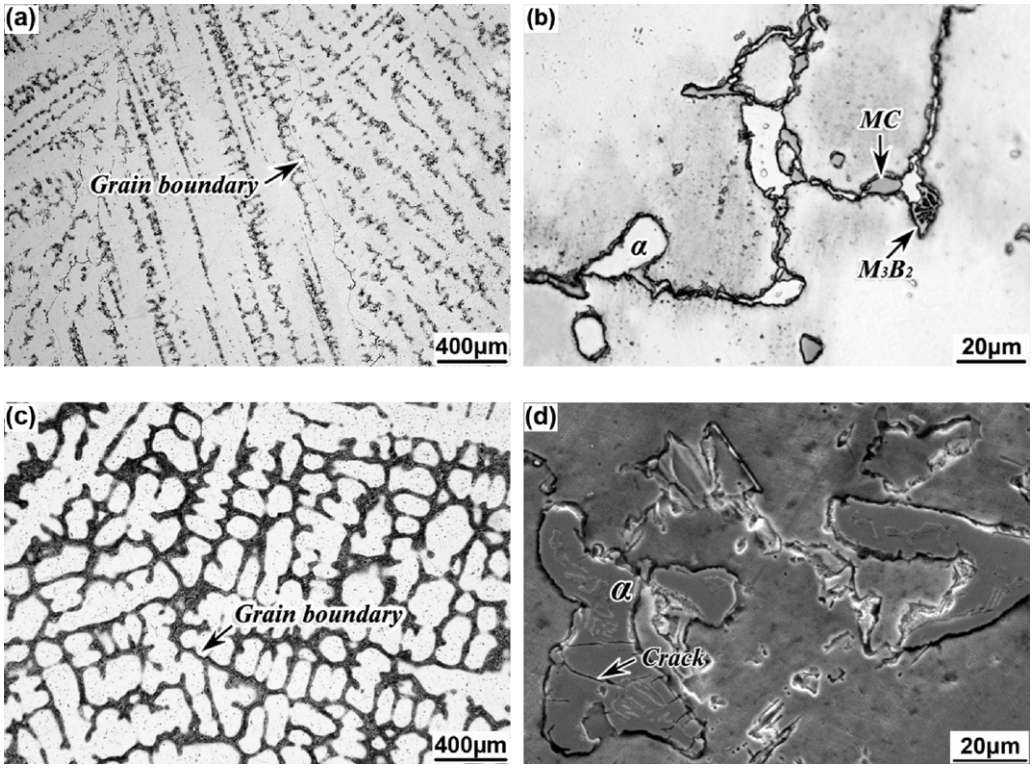

Fig. 1. The microstructure of as-cast K4648 alloy with different section size: (a) and (b) 10 × 10 mm, (c) and (d) 40 × 60 mm.

Table 2
Dendritic arm spacing, volume fraction and size of primary α phase in K4648 alloy with different section size.

Section size (mm)	Dendritic arm spacing (μm)	Volume fraction of primary α-(Cr,Ni) phase (vol.%)	Mean value of maximum diameter of primary α-(Cr,Ni) phase (μm)
10 × 10	66.7	0.64	17.5
40 × 60	110.9	1.29	56.0

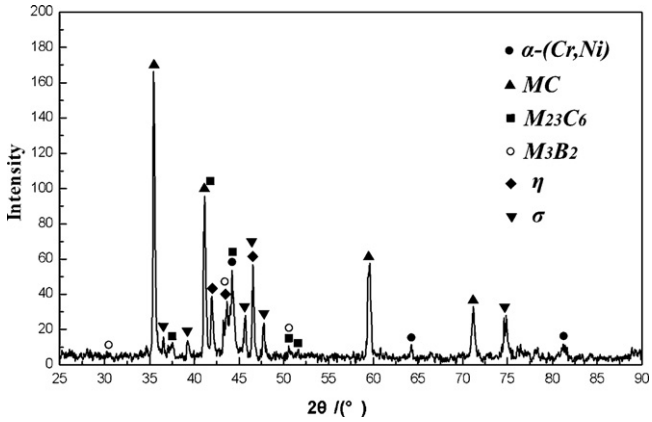

Fig. 2. X-ray diffraction pattern of the minor phases in as-cast K4648 alloy with section size of 40 × 60 mm.

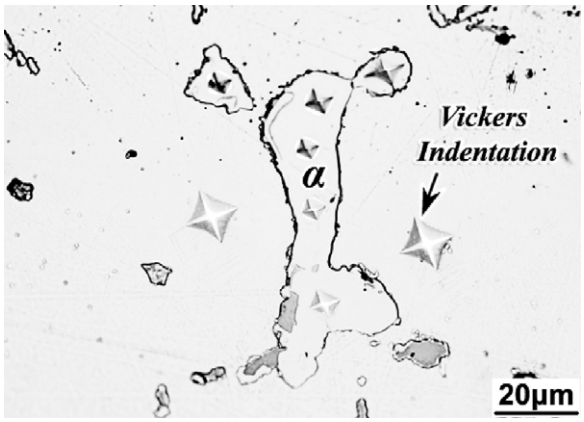

Fig. 3. Vickers microhardness test of primary α phase compared with that of the γ matrix in K4648.

distinct dendritic arm spacing for different section size samples. The casting with a section size of 40 × 60 mm possesses a dendritic arm spacing almost one time higher than that of the 10 × 10 mm impact testing bar (Fig. 1a and c). Under higher magnification, it is revealed that the blocky primary α phase, MC carbides, and occasional M_3B_2 borides are distributed in the interdendritic region and grain boundaries (Fig. 1b and d). The specimens with a large section size of 40 × 60 mm possess larger and more numerous α phase than do the 10 × 10 mm samples due to the slow solidification, which can be proved by the data in Table 2.

The X-ray diffraction measurements of extracted minor phases for large section specimen are shown in Fig. 2, and prove the existence of α phase (body-centered cubic solid solution), MC, $M_{23}C_6$ and M_3B_2. Small quantities of η and σ are also present due to the severe segregation during slow solidification.

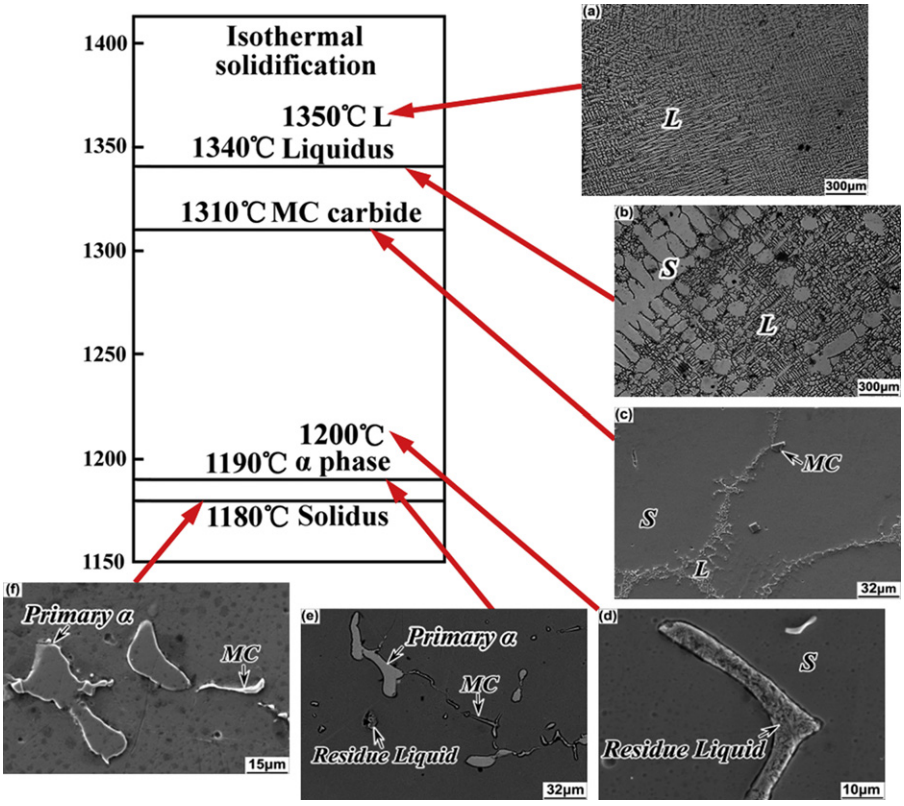

Fig. 4. Precipitated sequence of phases in liquidus and solidus temperature range of K4648 alloy (primary α phase precipitated at 1190 °C).

Table 3
Composition of primary α phase in different section size specimens of as-cast K4648 alloy (atomic fraction, %).

Section size (mm)	Cr	Ni	Mo	W	Ti
10 × 10	54.33	33.41	7.22	3.86	1.08
40 × 60	56.37	32.48	7.40	3.14	0.61

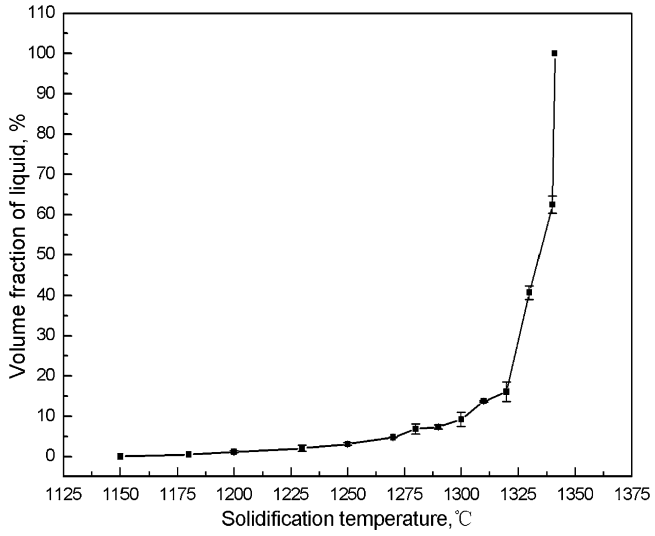

Fig. 5. Characteristic curve of solidification for K4648 alloy.

The compositions of primary α phases are listed in Table 3. The α phases consist mainly of elemental Cr and Ni, and small amounts of solutionized Mo and W. It was noteworthy that the concentration of elemental Ni in primary α phase can be as high as 30 at.%. Alpha phase can therefore be represented as α-(Cr, Ni). Based on the Ni—Cr binary phase diagram [24], the maximum solubility of Ni in Cr is 38 at.% at 1345 °C and Ni has almost no solubility in Cr below 600 °C. However, in this study, 32.48–33.41 at.% Ni, over 10 at.% total W plus Mo content solutionized in primary α phase, indicate that the primary α phase is an oversaturated solid solution phase.

The Vickers microhardness test at a load of 0.2 N was carried out, and the primary α phase possessed a hardness of 6.3 GPa, which was three times harder than that of γ matrix, which was 1.93 GPa (Fig. 3). Cracks present in large blocky primary α phases of as-cast heavy section casting (Fig. 1d), indicate that primary α phase is hard and brittle.

3.2. Formation of primary α phase

The isothermal solidification specimens was remelted at 1360 °C and held for 10 min, followed by water quenching cooling (ISQ) to determine the phase-specific precipitation temperatures and the liquid residual volume fraction. The solidification sequence for various phases of K4648 alloy are illustrated in Fig. 4. The solidified and unsolidified regions at different temperatures can be clearly distinguished by the coarse dendrites as solid (S) and ultra fine dendrites as liquid (L) (Fig. 4b). The frozen liquid fraction in the solidified specimens at different temperatures was plotted against solidification temperature as shown in Fig. 5.

It could be seen that the primary α phase did not form as the temperature decreased to 1200 °C (Fig. 4d). The onset of the primary α phase precipitation took place at 1190 °C (Fig. 4e) from very small amount of residual liquid (about 1 vol.%, Fig. 5). Script-like fine MC carbides formed in residual liquid region after quenching at 1310 °C with a residual liquid volume fraction of 13.7 vol.% (Figs. 5 and 6a). Moreover, small amounts of blocky fine quenched α phase began to precipitate accompanied by the formation of fine MC carbides in the residual liquid region at 1290 °C (Figs. 5 and 6b) as the residual liquid volume fraction decreased to 7.4 vol.%. The composition of frozen residual liquid at 1290 °C, 1200 °C and α phase at 1190 °C compared with that of the bulk alloy are listed in Table 4 (Table 1, Figs. 4d and e, 6b). The concentration of Cr in the residual liquid region increased with decreasing temperature during solidification. The Cr level in the residual liquid at 1200 °C can reach up to 51 at.%, which is close to the composition of primary α-(Cr,Ni) phase (Table 4), and the α phase precipitate at 1190 °C. Therefore, the continuous segregation of elemental Cr in the residual liquid during solidification resulted in the formation of primary α phase.

3.3. Solid solution and transformation of primary α phase

The specimens cut from the thin section testing bars and heavy section castings were solid solutionized at 1180 °C, 1200 °C and 1220 °C for 1 h, the microstructures were shown in Fig. 7. During the solid solution treatment of K4648 alloy at temperatures above 1180 °C, small size primary α phase solutionized, larger primary α phase transformed into $M_{23}C_6$ carbides (Fig. 7a–d). The $M_{23}C_6$ carbides has been reported to be formed through the reaction $MC + \gamma \rightarrow M_{23}C_6 + \gamma'$ previously [25]. However, in this investigation,

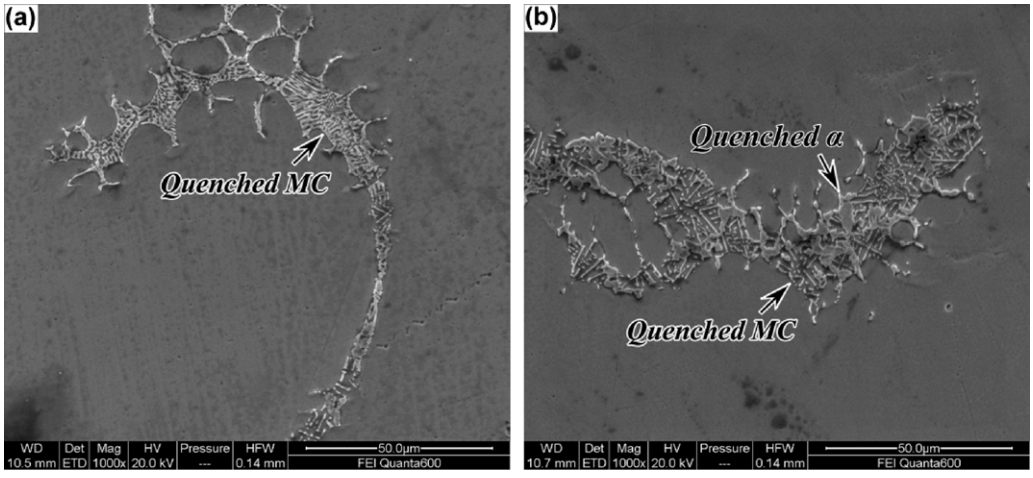

Fig. 6. Quenching microstructures of K4648 alloy after isothermal solidification at different temperatures: (a) 1310 °C, no quenched α phase, (b) 1290 °C, quenched α phase exists.

Table 4
The concentration of elemental Cr in the residual liquid region and in the primary α phase in K4648 alloy (atomic fraction, %).

	Cr	Ni	Mo	W	Ti	Al	Nb
Bulk alloy	37.55	55.16	1.75	1.53	1.11	2.02	0.56
Residual liquid at 1290 °C	44.27	39.79	4.66	2.39	3.36	1.10	4.42
Residual liquid at 1200 °C	51.36	38.93	4.64	2.83	1.10	0.86	–
Primary α phase at 1190 °C	55.13	34.48	6.11	3.46	0.81	–	–

the reaction of α-(Cr,Ni) + C → $M_{23}C_6$ occurred through the in situ a phase absorbed carbon. It was evident that the primary α phase obviously solutionized as the temperature was held at 1180 °C for 1 h. The solutionized α phase increased with increasing temperature (Fig. 7). Finally, at 1220 °C/1 h, almost all primary α phase solutionized or transformed into $M_{23}C_6$ carbides (Fig. 7e and f). Moreover, incipient melting occurred at a temperature range of 1200–1220 °C. In superalloys, the incipient melting often occurs during high temperature heat treatment [26]. After solution etching with 10 g potash prussiate + 10 g NaOH + 100 ml H_2O, the primary α phase exhibited line etching and green or pink color in optical metallography, compared with the gray color of $M_{23}C_6$ carbides (Fig. 7a–d). This color difference can be used to distinguish these two phases in quantitative metallography. The volume fraction of primary α phase in as-cast and in different temperature solid solution treated specimens are shown in Fig. 8, and reveal that the amount of primary α phase decreased with increasing the solution temperature. It was evident that the volume fractions of primary α phase in faster cooled thin section testing bars were much lower than that in slow-cooled heavy section castings at corresponding solid solution temperatures. Therefore, the faster cooling during solidification process can decrease the amount of primary α phase in both as-cast and heat-treated K4648 alloys.

Standard solid solution heat treatment of 1180 °C/4 h was performed both on the 10 × 10 mm and 40 × 60 mm specimens, and the results were illustrated in Fig. 9. In thin section specimen, some

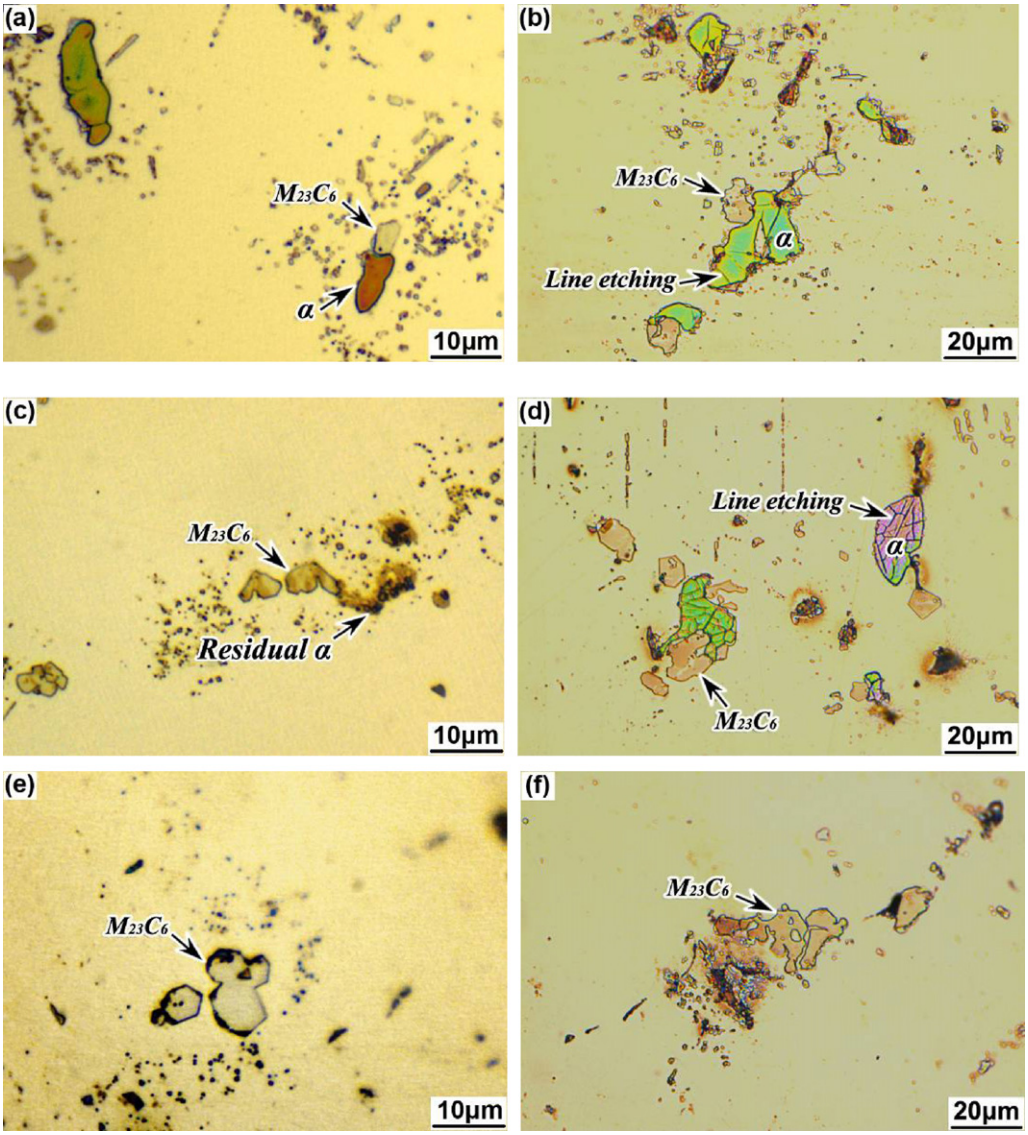

Fig. 7. Microstructures of K4648 alloy with different section size after different temperatures of solid solution treatment: (a) 1180 °C/1 h, 10 × 10 mm, (b) 1180 °C/1 h, 40 × 60 mm, (c) 1200 °C/1 h, 10 × 10 mm, (d) 1200 °C/1 h, 40 × 60 mm, (e) 1220 °C/1 h, 10 × 10 mm, (f) 1220 °C/1 h, 40 × 60 mm.

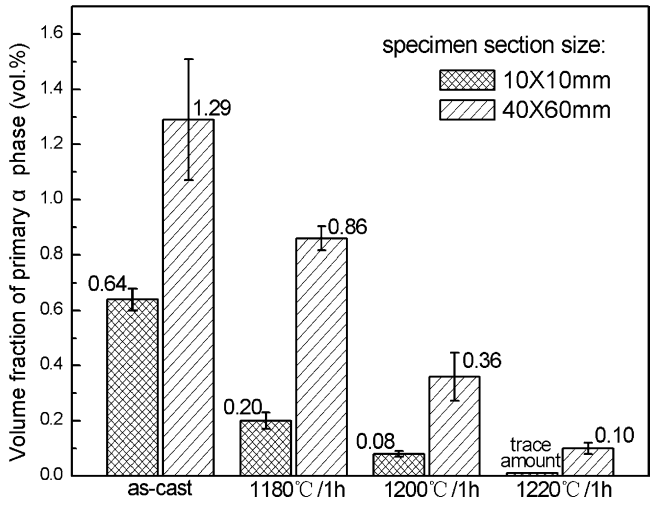

Fig. 8. The volume fraction of primary α phase in K4648 at different solid solution temperatures.

primary α phase transformed into regular shaped $M_{23}C_6$ carbides in situ, others solid solutionized. Furthermore, small granular $M_{23}C_6$ precipitated from the γ matrix at the periphery of transformed blocky $M_{23}C_6$ carbides (Fig. 9a). However, large blocky primary α phase only partially transformed into $M_{23}C_6$ carbides in large section specimens after 1180 °C/4 h treatment (Fig. 9b). It was noteworthy that the primary α phase and transformed $M_{23}C_6$ carbides exhibit a network-like distribution in heavy section specimens, whereas they have a more uniform and isolated distribution in the faster cooled thin section specimens.

The compositions of residual α phase and transformed $M_{23}C_6$ carbides in specimens with different section sizes are listed in Table 5. It can be concluded by comparing the data in Tables 3 and 5 that the solid solution treated specimens possess similar compositions of the residual α phase to those of as-cast specimens. It was noteworthy that the $M_{23}C_6$ carbide possesses as much higher content of Cr and less Ni than did the primary α phase. In summary, after solid solution treatment in the 1180–1220 °C range, the primary α phase solutionized or transformed into more brittle $M_{23}C_6$ carbides. Moreover, the volume fraction of primary α phase decreased with increasing the solution temperature.

3.4. The effect of primary α phase on the impact ductility of K4648 alloy

The impact testing bars were cut from 10 × 10 mm shaped bar and 40 × 60 mm casting with a 1180 °C/4 h + 900 °C/16 h standard heat treatment. The impact ductility of specimens at ambient temperature are shown in Fig. 10. The result indicated that the impact ductility of thin section specimen was twice as high as that of heavy section samples. The impact ductility of slow-cooled heavy section specimens did not meet the K4648 specification minimum

Table 5
Composition of phases in K4648 alloy after solution treatment at 1180 °C/4 h (atomic fraction, %).

Section size (mm)	Phases	Ti	Cr	Ni	Mo	W
10 × 10	Primary α	0.66	55.25	34.79	5.64	3.66
	$M_{23}C_6$	0.19	82.28	8.60	5.35	3.59
40 × 60	Primary α	0.39	54.03	34.03	7.45	4.09
	$M_{23}C_6$	0.09	84.33	6.11	5.67	3.80

Note: The content of carbon in $M_{23}C_6$ was not determined.

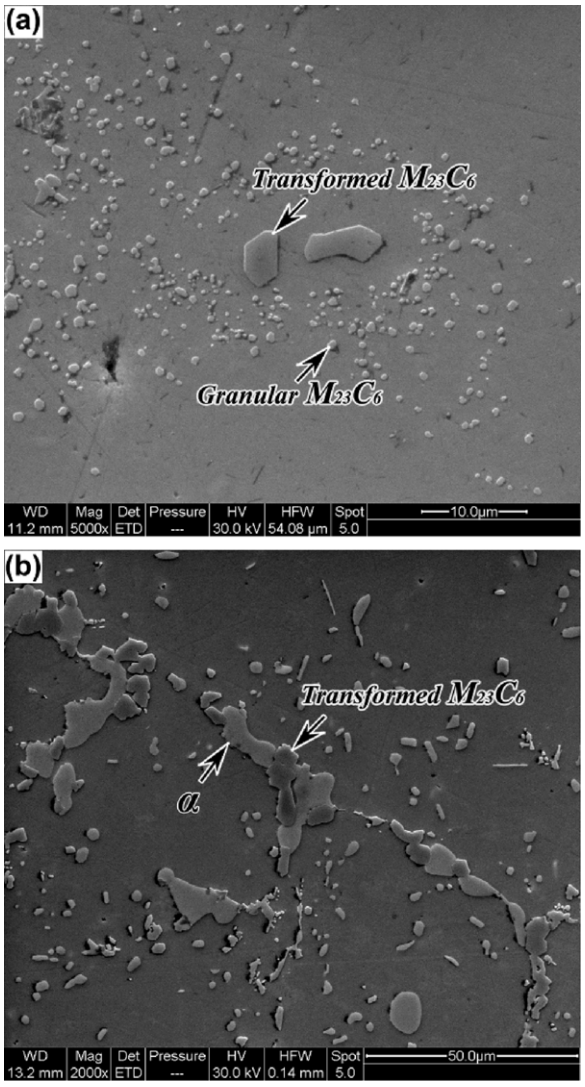

Fig. 9. Microstructures of K4648 alloy with different section size after standard solid solution treatment: (a) 1180 °C/4 h, 10 × 10 mm, (b) 1180 °C/4 h, 40 × 60 mm.

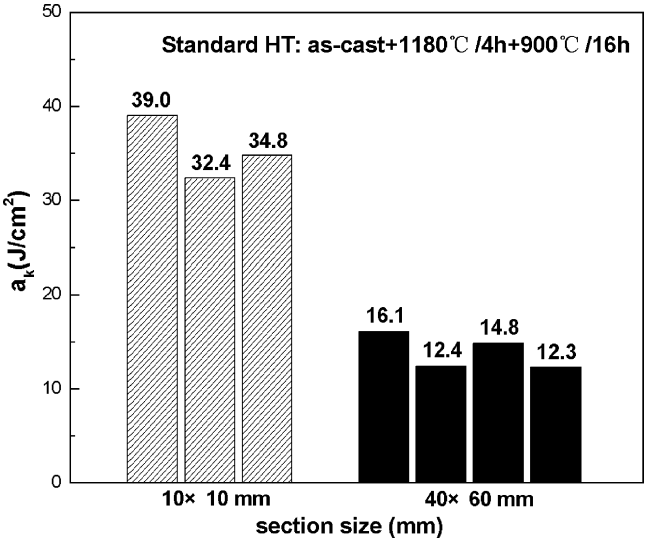

Fig. 10. The impact ductility (a_{ku}) of different section size specimens for K4648 alloy with standard heat treatment (K4648 specification requirement: $a_{ku} \geq 19.6$ J/cm^2).

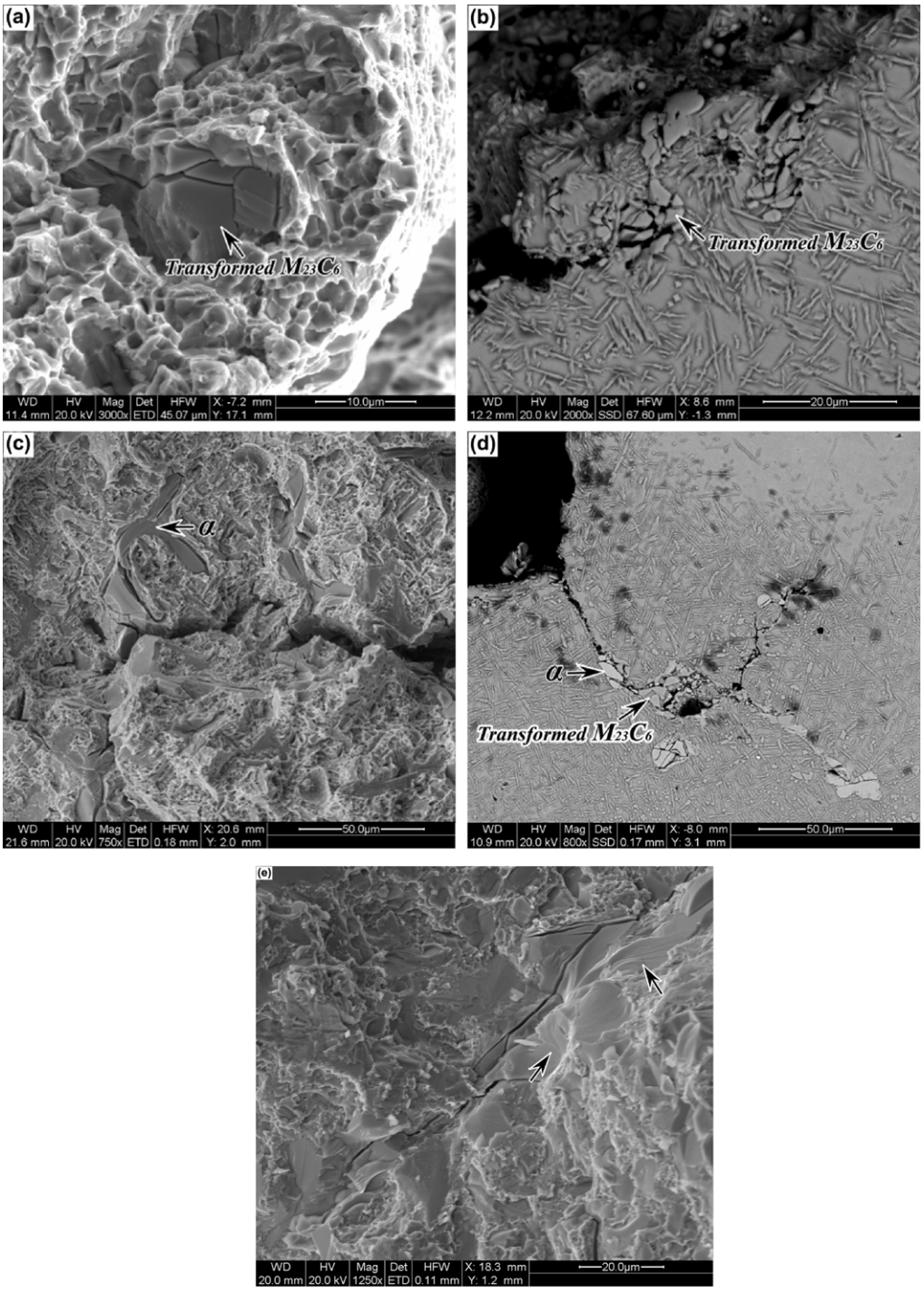

Fig. 11. Morphology of fracture surface (a), (c), and (e) and microstructure of longitudinal section (b) and (d) of impact specimens with different section size: (a) and (b) 10 × 10 mm, (c), (d), and (e) 40 × 60 mm.

Table 6
The compositions of phases in the fracture surface and longitude section of specimens of K4648 alloy with different section size.

Specimens original section size	Position	Phases	Cr	Ni	Mo	W
10 × 10 mm	Fracture surface	$M_{23}C_6$	82.95	6.72	5.07	5.26
	Longitudinal section near the fracture surface	$M_{23}C_6$	82.24	6.39	5.87	5.51
40 × 60 mm	Fracture surface	Primary α	54.57	32.98	7.66	4.78
	Longitudinal section near the fracture surface	Primary α	54.38	34.21	7.01	4.40
		$M_{23}C_6$	82.73	6.60	5.83	4.85

Note: The content of carbon in $M_{23}C_6$ was not determined.

requirement of 19.6 J/cm^2. A micrograph of fracture surface and longitudinal section of the impact ductility specimens are shown in Fig. 11. Extensive cracks appeared in brittle primary α phase and the transformed $M_{23}C_6$ carbides (Fig. 11a, c, and e) on the fracture surface. Brittle fractures occurred in slower cooled heavy section specimens. Under higher magnification, a "river pattern" structure is obvious in regions marked by arrows in Fig. 11e. The river pattern appearance is the main feature of the cleavage fracture. Additionally, secondary cracks formed at these phases and the interfaces of α/matrix or $M_{23}C_6$/matrix, especially in heavy section samples (Fig. 11c and d). It can be seen by comparing Fig. 11c and d with Fig. 9b that a network-like distribution of brittle primary α phase and the transformed $M_{23}C_6$ carbides was evident in slow-cooled heavy section specimens and secondary cracks were prone to propagate at these continuous distributed brittle phases (Fig. 11c and d). In contrast, cracking of the small carbides formed at a faster cooling rate was contained by surrounding ductile γ matrix (Fig. 11a and b). The compositions of cracked phases were detected by EDS and the results are listed in Table 6. Comparing the data in Tables 5 and 6, the compositions of phases are similar, indicating that the cracked phases are primary α phase and transformed $M_{23}C_6$ carbides.

The impact ductility of the K4648 alloy related to the size, volume fraction and the distribution of primary α-(Cr,Ni) phase. It can be concluded that the large amount and size of blocky primary α phase with a network-like distribution formed at slower cooling rate during solidification process in heavy section specimens should be responsible for the lower impact ductility of the high Cr content K4648 alloy. As mentioned above, it was difficult to completely solid solutionized the large blocky primary α phase, which tended to transform into the more brittle $M_{23}C_6$ carbides, with both phases resulting in diminished ductility. Therefore, proper parameter to obtain faster cooling in the solidification of the alloy must be considered to avoid the detrimental primary α phase precipitation.

4. Conclusions

1. Primary α-(Cr,Ni) phase exists in the as-cast microstructure of K4648 alloy. It is an oversaturated solid solution of Ni, Mo and W in Cr. The concentration of elemental Ni can reach more than 30 at.%. At a load of 0.2 N, α-(Cr,Ni) phase possesses a vickers microhardness of 6.3 GPa. It is hard and brittle and tends to crack in both as-cast and heat treated alloy.
2. The onset of the primary α-(Cr,Ni) precipitation took place at 1190 °C at late solidification from very small amounts of residual liquid (about 1 vol.%) in the interdendritic region and grain boundaries, and was caused by the continuous segregation of Cr during the solidification process.
3. The primary α phase solid solutionized and transformed into $M_{23}C_6$ carbides in the range of 1180–1220 °C. Incipientmelting occurred in the 1200–1220 °C range. The volume fraction of primary α phase decreased with increasing the solid solution temperature. The faster cooling during solidification process can decrease the amount of primary α phase in both as-cast and heat-treated K4648 alloys.
4. Extensive cracked α phase or transformed $M_{23}C_6$ carbides can be observed at the fracture surfaces and longitudinal sections of impact specimens and led to decrease impact ductility of high Cr content cast Ni-base superalloy K4648. Brittle fractures occurred in slower cooled heavy section castings specimens due to the existence of large amounts and sizes of blocky primary α-(Cr,Ni) phase with a network-like distribution. It was difficult to remove this phase by heat treatment. Therefore, the parameter control during the solidification process of alloy is significant, and faster cooling becomes an effective method to avoid the detrimental large blocky primary α phase precipitation.

References

[1] C.T. Sims, N.S. Stoloff, W.C. Hagel, Superalloys II, Wiley-Interscience, New York, 1987.
[2] S. Tin, T.M. Pollock, J. Propul. Power 22 (2006) 361–374.
[3] A. Picasso, A. Somoza, A. Tolley, J. Alloys Compd. 479 (2009) 129–133.
[4] A.V. Shulga, J. Alloys Compd. 436 (2007) 155–160.
[5] J.Y. Chen, Q. Feng, Z.Q. Sun, Scr. Mater. 63 (2010) 795–798.
[6] F. Long, Y.S. Yoo, C.Y. Jo, S.M. Seo, H.W. Jeong, Y.S. Song, T. Jin, Z.Q. Hu, J. Alloys Compd. 478 (2009) 181–187.
[7] G. Liu, L. Liu, C. Ai, B. Ge, J. Zhang, H. Fu, J. Alloys Compd. 509 (2010) 5866–5872.
[8] X.B. Zhao, L. Liu, C.B. Yang, Y.F. Li, J. Zhang, Y.L. Li, H.Z. Fu, J. Alloys Compd. 509 (2011) 9645–9649.
[9] Y. Gu, T. Fukuda, C. Cui, H. Harada, A. Mitsuhashi, T. Yokokawa, J. Fujioka, Y. Koizumi, T. Kobayashi, Metall. Mater. Trans. A40 (2009) 3047–3050.
[10] Q. Zeng, S.W. Ma, Y.R. Zheng, S.Z. Liu, T. Zhai, J. Alloys Compd. 480 (2009) 987–990.
[11] J. Mi, P.S. Grant, Acta Mater. 56 (2008) 1597–1608.
[12] X.F. Yan, H.P. Ma, Y.X Lu, J. Mater. Eng. 3 (2002) 26–29.
[13] H.P Ma, Y.J. Yang, X.F. Yan, J. Iron Steel Res. 19 (2007) 54–57.
[14] J.X. Dong, X.S. Xie, Acta Metall. Sin. 41 (2005) 1159–1166.
[15] M. Terada, M.F. Hupalo, I. Costa, A.F. Padilha, J. Mater. Sci. 43 (2008) 425–433.
[16] G.L. Wang, C.W. Wu, M.C. Zhang, J.X. Dong, X.S. Xie, Rare Metal Mater. Eng. 31 (2002) 37–40.
[17] J.F. Radavich, in: E.A. Loria (Ed.), Superalloy 718, 625, 706 and Various Derivatives, TMS, Warrendale, PA, 1997, pp. 409–415.
[18] K.Y. Cheng, D.H. Kim, Y.S. Yoo, C.Y. Jo, T. Jin, Z.Q. Hu, J. Mater. Sci. Technol. 24 (2008) 127–130.
[19] L. Zheng, Scr. Mater. 53 (2005) 943–948.
[20] L. Zheng, Scr. Mater. 50 (2004) 435–439.
[21] X. Wang, Y. Zheng, C. Xiao, B. Wang, Y. Han, Trans. Nonferrous Met. Soc. China 10 (2000) 430–434.
[22] Y. Zheng, L. Zhao, K. Tangri, J. Mater. Sci. 28 (1993) 823–829.
[23] Y. Zheng, C. Li, D.N. Duhl, G. Maurer, S. Antolovich, C. Lund, S. Reichman, Superalloys 1988, TMS, Warrendale, PA, 1996, pp. 475–484.
[24] http://www.calphad.com/nickel-chromium.html.
[25] C.N. Wei, H.Y. Bor, L. Chang, J. Alloys Compd. 509 (2011) 5708–5714.
[26] O.A. Ojo, N.L. Rechards, M.C. Chaturvedi, J. Mater. Sci. Lett. 39 (2004) 7401–7404.